Comprehensive simulation of a complete tiltrotor with pilot-in-the-loop for whirl-flutter stability analysis

Alessandro Cocco *, Alberto Savino, Andrea Zanoni, Pierangelo Masarati

Politecnico di Milano, Milano - Italy

* alessandro.cocco@polimi.it

Abstract

This work presents the complete aero-servo-elastic model Bell XV-15 tilt-rotor equipped with Advanced Technology Blades (ATB). Multibody and aerodynamic modeling of each subcomponent, using the open-source software MBDyn and DUST, is illustrated and validated considering experimental and numerical results. The design of optimal longitudinal control of the tilt-rotor is presented and validated. Finally, the detailed biomechanical pilot model is coupled with the aeroelastic tiltrotor model. To evaluate the capability of the model to evaluate the aeroelastic stability a is evaluated through a frequency sweep excitation of the model during a time-marching simulation, and the principal airframe modes are identified through the Matlab system identification. This model opens a wide spectrum of different analyses that could be performed, for example, this model will be use to study passengers' comfort, performances in transient maneuvers such as conversion and pull-up, aeroelastic stability, pilot-induced-oscillation phenomena. Due to the modularity and parameterization of the model, other innovative VTOL configurations could be studied with the purposed approach.

1 INTRODUCTION

Tiltrotor aircraft provide the ability to take off and land vertically like a helicopter while reaching high-speed forward flight. It is one of the few successful examples of advanced vertical lift configurations.

After a long development phase with several experimental aircraft, for example, the Bell XV-15 [1], the concept finally proved its feasibility with the military aircraft Bell-Boeing V-22 [2]. Looking at the civil market, the originally Bell-Agusta and now Leonardo AW609 [3] is about to become operational after a long and thorough development [4], proving that the tiltrotor design appears to be mature enough to enter also the civilian market [5].

However, tilt-rotor design remains a rather challenging engineering task considering the various operating conditions and multi-purpose missions that are expected to be accomplished by such a complex type of aircraft. In particular, the problem of assessing whirl-flutter stability limits is at the same time fundamental and challenging. Whirl flutter is an aeroelastic instability phenomenon that can affect both turboprop and tilt-rotor aircraft [6]. The difficulty lies in its dependence on several factors, including the geometrical design, structural properties, the dynamics of the actuators and flight control system, unsteady interactional aerodynamics, and the pilot-in-the-loop, which can all contribute to the whirl-flutter characteristics in ways that are not always intuitive. The problem may be exacerbated when unconventional configurations are considered, as is the case for advanced air mobility concepts driven by propellers and rotors [7].

A comprehensive tool that can accurately predict this aeroelastic phenomenon that takes into account all the previously mentioned participants is of paramount importance from an industry standpoint, since aeroelastic testing, especially when it concerns stability and flutter, can be extremely dangerous.

This work, following previous modeling efforts on full-scale tilt-rotor multibody modeling [8, 9, 10], aims to provide a numerical environment capable of taking into account all the main players in whirl-flutter. Thanks to a large amount of data available [11, 12] a full flexible multibody model of the XV-15 tiltrotor has been built using the free software MBDyn(https://mbdyn.org/) [13]. To model the wing/blade aerodynamics, two levels of fidelity were used. The simpler model is based on 2D strip theory and is available in MBDyn. The other model is based on a mid-fidelity approach that takes advantage of a solution to the aerodynamic problem based on the vortex particle method implemented in DUST (https://www.dust-project.org/) [14]. The coupling between MBDyn and DUST is validated and presented in [15].

Finally, pilot biomechanics is introduced into the simulation environment using the multibody pilot model presented in [16]. The airframe eigenmodes have been extracted using a frequency sweep approach trying to reproduce flight test campaign presented in [17] and identified using a time-to-frequency domain approach as was used in [18].

2 NUMERICAL TOOLS

2.1 MBDyn

MBDyn (https://mbdyn.org/) [13] is a free general-purpose multibody solver, developed at the Aerospace Science and Technology department of Politecnico di Milano.

MBDyn automatically writes and solves the equations of motion of a system of entities possessing degrees of freedom (nodes) connected through algebraic constraints and subjected to internal and external loads. Constraint equations are explicitly accounted for, following a redundant coordinate set approach. Thus, the resulting system of differential-algebraic equations (DAEs) takes the Hessenberg form.

$$(1a) \qquad \mathbf{M}(\mathbf{x},t)\dot{\mathbf{x}} = \mathbf{p}$$

$$(1b) \qquad \dot{\mathbf{p}} = \phi_{/\mathbf{x}}^{T}\lambda + \mathbf{f}_i(\dot{\mathbf{x}},\mathbf{x},t) + \mathbf{f}_e(\dot{\mathbf{x}},\mathbf{x},t)$$

$$(1c) \qquad \mathbf{0} = \phi(\mathbf{x})$$

where $\mathbf{x}$ is the vector of the kinematic unknowns, $\mathbf{p}$ that of the momentum unknowns, λ that of the algebraic Lagrangian multipliers, $\mathbf{M}$ is a configuration- (and possibly time-)dependent inertia matrix, vectors $\mathbf{f}_i$ and $\mathbf{f}_e$ contain generalized internal and external forces, $\phi(\mathbf{x})$ is the vector of the (typically nonlinear) algebraic equations that express kinematic holonomic constraints, and $\phi_{/\mathbf{x}}$ is the Jacobian matrix of the constraints with respect to the kinematic unknowns.

Each node instantiates the corresponding balance equations (1b); nodes with associated inertia properties also instantiate the related momenta definitions (1a).

Additional states associated with scalar fields (e.g., hydraulic pressure, temperature, electric potential), and thus the corresponding balance equations, are accounted for thanks to dedicated node types.

Elements are responsible for the contributions to the balance equations through (visco-)elastic, internal forces $\mathbf{f}_i$, possibly state-dependent external force fields $\mathbf{f}_e$ (e.g., aerodynamic forces), and reaction forces $\mathbf{f}_c = \phi_{/\mathbf{x}}^{T}\lambda$, introduced using the Lagrange multipliers λ and the Jacobian matrix of the algebraic constraint equations in Eq. (1c).

The DAE system can be integrated using different stable A / L integration methods, among which is an original multistep one with tunable algorithmic dissipation, specifically designed for the class of problems usually solved with MBDyn [19].

2.2 DUST

DUST is an open-source software developed by Politecnico di Milano since 2017 for the simulation of the interactional aerodynamics of unconventional rotorcraft configurations. The code is released as free software, under the open-source MIT license (https://www.dust-project.org/). The code relies on an integral boundary element formulation of the aerodynamic problem and on a vortex particle model [20, 21] of the wakes. A numerical model in DUST can be built using several components, connected to user-defined reference frames, whose position and motion can be defined in a hierarchical way. The presence of different aerodynamic elements allows for different levels of fidelity in the model, ranging from lifting line elements to zero-thickness lifting surfaces and surface panels for thick solid bodies. The simulation evolves in time with a time-stepping algorithm, solving in sequence the Morino-like problem [22] for the potential part of the velocity field, the nonlinear problem for the lifting lines, and updating the rotational part of the velocity field by integrating the Lagrangian dynamical equations of the wake particles. A detailed description of the mathematical formulation implemented in DUST is reported in [23].

3 XV-15 AEROELASTIC MODEL

In the present work, a detailed aeroservoelastic model of the XV-15 tiltrotor with Advanced Technology Blade (ATB) was built to obtain a numerical model suitable for investigating the phenomenon of whirl flutter. The model consists of the following components:

1. Rotors aeroelastic model

2. Simplified drive system

3. Fixed airframe stick model

4. Vortex particle aerodynamic of rotor and wing surfaces
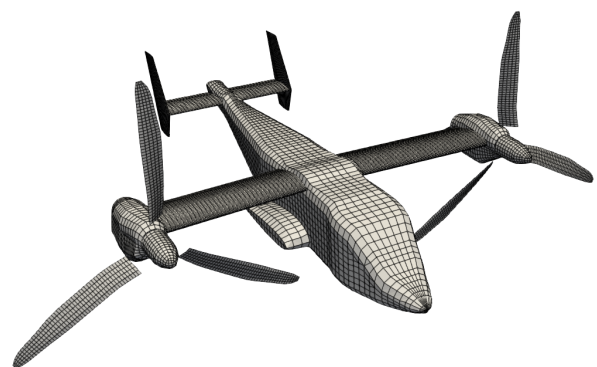
5. Detailed biomechanical model of the pilot's upper body

Figure 1: XV-15 DUST aerodynamic mesh equipped with ATB blades

3.1 ROTOR MODEL

The multibody model of the XV-15 proprotor is made up of ATB blades. The rotor is stiff in plane with a gimballed hub.

Based on the information provided by [11], the layout of a control chain representative of that of the XV-15 proprotor shown in Fig. 2 was modeled.
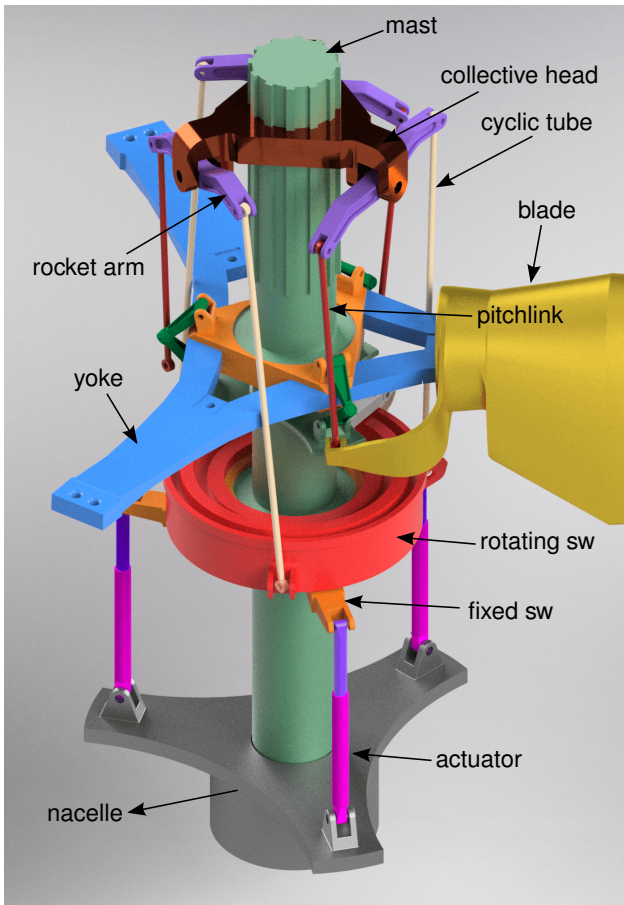

Figure 2: Layout of the XV-15 proprotor control chain.

Concerning the elastic part, the blades and yoke are modeled using the MBDyn finite-volume beam element [24, 25]. A total of 12 beam elements were used for each blade and 5 for the yoke to match the first seven collective and cyclic rotor modes.

To model the blade aerodynamics, two levels of fidelity were used. The simpler model is based on 2D strip theory and is available in MBDyn using a dynamic input model. A second, more sophisticated, model relies on DUST nonlinear vortex lattice elements. To take into account the interactional effects between the different aerodynamic bodies, the wing and tail empennages are modeled using 3D surface panels with a vortex particle wake. The complete aerodynamic mesh is represented in Fig. 1.

3.2 ROTOR VALIDATION

The results presented in this work are mainly related to the validation of the model to demonstrate its usability as a testbed for future research and analysis. Moreover, this complete validation is intended to be a solid base for other code-to-code validation, that, to the authors' knowledge, is still not published with this level of detail. The validation of the rotor from the dynamic structural point of view and in terms of aerodynamic performance is presented. Then, the analysis of the drive system and the airframe are presented.

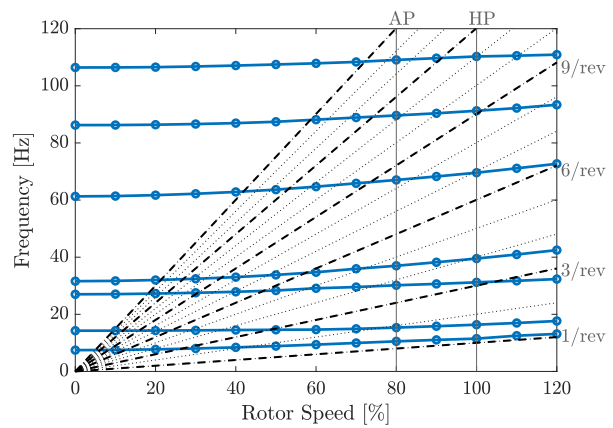### 3.2.1 ROTOR CAMPBELL DIAGRAM

Figure 3: Rotor Campbell diagram in vacuum at collective pitch of 40°: collective Modes
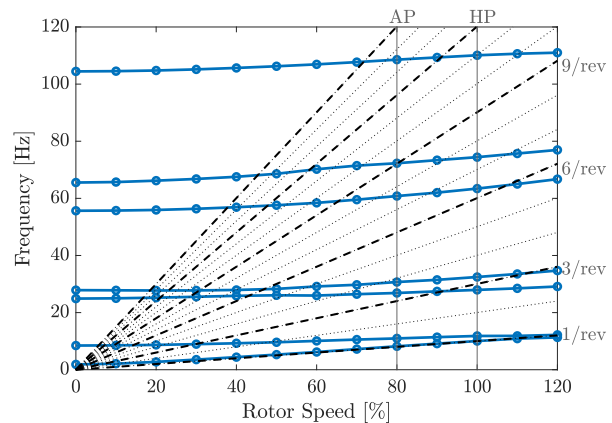

Figure 4: Rotor Campbell diagram in vacuum at collective pitch of 40°: cyclic modes

The isolated rotor dynamic behavior in vacuum is validated by means of the Campbell diagram. In these diagrams, the rotational frequency of each mode shape is tracked against the rotor speed. Each Campbell diagram has been calculated considering different rotor speed and evaluating the eigenvalues using Arpack library [26] and the eigenvalue card present in MBDyn [27]. Figures 3 and 4 shows the results considering a collective angle of 40° for collective modes and cyclic modes, respectively.

A detailed comparison between CAMRAD-JA and MBDyn models is presented in Table 1. Good agreement is visible in both collective and cyclic modes. The most noticeable difference can be seen in the first torsion mode. This can be explained by the fact that in the CAMRAD-JA

the control chain is modeled as a conventional helicopter-like control chain with a single control path, whereas in the MBDyn model it is modeled with a dual load path. The pitch mode is very close to the 3/rev. When flown in forward helicopter mode, this 3/rev aerodynamic excitation coupled with the natural frequency of the system produced high structural loads [1].

3.2.2 ROTOR POLAR

To validate the results of the rotor hover performance, comparing the numerical results with the experimental data reported in [28]. The results are presented in Figs. 5 and 6. It is clear that the simple 2D aerodynamic model that is present in MBDyn captures, almost correctly, the thrust; whereas the torque is overestimated in all collective ranges. This limitation can be overcome by coupling the MBDyn structural model with the DUST mid-fidelity aerodynamic code, which employs a more sophisticated vortex particle wake model.
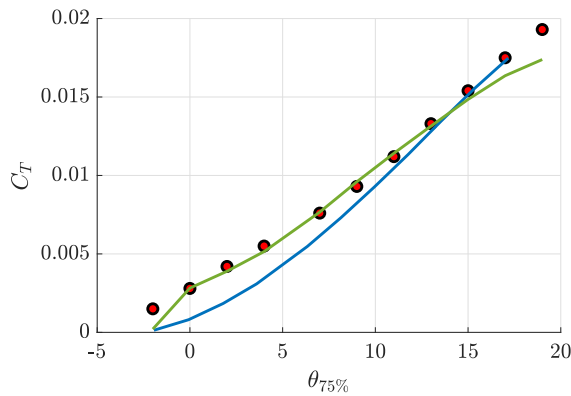

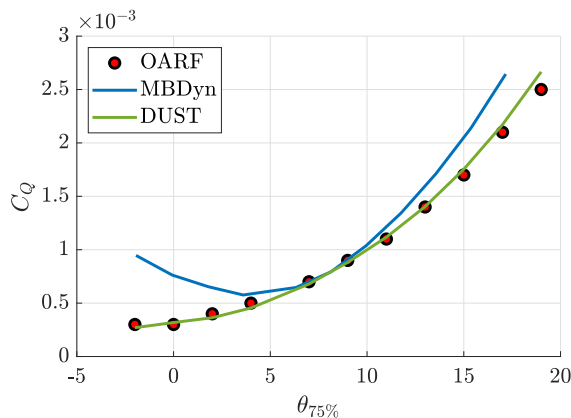Figure 5: Rotor hover results: thrust coefficient (C_T) vs collective pitch angle

Figure 6: Rotor hover results: torque coefficient (C_Q) vs collective pitch angle

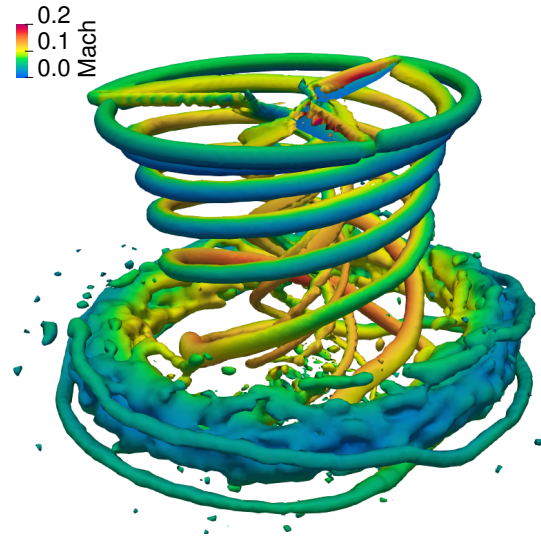

Figure 7: Wake visualization of the XV-15 ATB proprotor in hover by means of iso-surfaces of Q-criterion computed by DUST colored by Mach number.

3.3 DRIVE SYSTEM

In this work, a simplified model of a symmetric drive train system is proposed. Its scheme is shown in Fig. 8. The XV-15 engine model is derived from [11]: The engines are approximated as lumped inertia, while the rotor nodes do not have any inertia, as it is already included in the MBDyn models of the rotors. The two gearboxes are joined by an interconnecting shaft modeled with a torsional spring. The stiffness value of the torsional spring and engine inertia is reported in [11].

Each gearbox is modeled by two gimbal joints that impose the same angular velocity through each shaft. This arrangement provides redundancy to the loss of one engine since it permits power transfer for transient conditions and provides rotational speed synchronization.

Figure 8: Flowchart of the MBDyn model of the XV-15 drive system
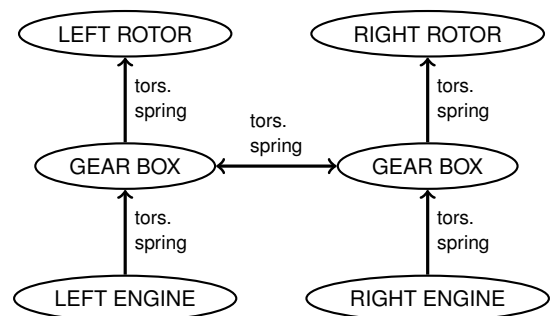
The validation has been carried out by comparing the frequency of the three modes of the system, as shown in Table 2.

Table 1: Frequency (Hz) comparison in non-rotating frame of the first 4 rotor modes in vacuum at 40° collective in AP mode

	CAMRAD-JA			MBDyn		
Mode	Collective	Regressive	Progressive	Collective	Regressive	Progressive
Gimbal	–	0.24	16.27	–	0.05	16.25
First Lag	10.19	2.42	18.45	10.53	2.83	19.10
First Flap	15.94	22.85	38.88	15.35	22.57	38.83
First Torsion	28.87	20.44	36.47	30.75	18.74	35.72

Table 2: Drive system modes frequency (Hz) comparison

Mode	[29]	MBDyn	Diff.
First anti-symmetric	4.50	4.50	0.18%
First symmetric	13.98	13.99	0.05%
Second anti-symmetric	16.62	16.59	−0.19%

Table 3: Airframe modes frequency (Hz) comparison

Mode	[12]	MBDyn	Diff.
Symmetric beam	3.33	3.34	0.24%
Symmetric chord	6.32	6.13	−3.08%
Symmetric torsion	8.38	8.31	−0.81%
Anti-symmetric beam	6.43	6.22	−3.36%
Anti-symmetric chord	8.76	8.80	0.51%
Anti-symmetric torsion	7.15	7.02	−1.81%

3.4 AIRFRAME

The airframe model has been developed to reproduce the fundamental frequencies and mode shapes of the full aircraft with respect to the wing-nacelle part. Stiffness and inertial data are taken from the Finite Element Model (FEM) model presented in [12]. The model is tuned to capture the six lowest normal modes of the wing-nacelle system: symmetric/anti-symmetric wing bending (SWB/AWB), symmetric/anti-symmetric wing chord (SWC/AWC) and symmetric/anti-symmetric wing torsion (SWT/AWC).

In MBDyn, the wing model is made of 5 finite-volume three-node beam elements and a set of lumped masses as for blades and yoke. The nacelle is considered a rigid body, connected to the wing by deformable joints that represent the flexibility of the down-stop attachment. The downstop stiffness varies as a function of the conversion angle ϕ; it is calculated following the approach presented in [29]. Control surfaces are modeled as rigid bodies, with associated polar inertia, and attached to the fixed-wing part by a statically determined constraint that is a combination of a spherical and inline joint. The fuselage has been modeled as a rigid body that transports the pilot seat, landing gears, horizontal and vertical empennages, and the wing-nacelle system. Aerodynamics is modeled by the MBDyn/DUST coupling presented in [15]. This allows the introduction of aerodynamic control surfaces to perform aeroelastic trim analysis, flutter stability analysis, and transient manoeuvres of the full aircraft.

The validation of the dynamics has been performed comparing the frequency of the first three symmetric and anti-symmetric wing modes in downstop-ON condition, concerning the original model proposed in [12]. The results are reported in Table 3.
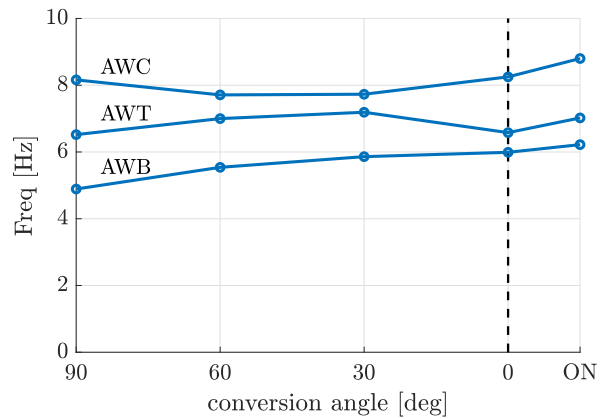

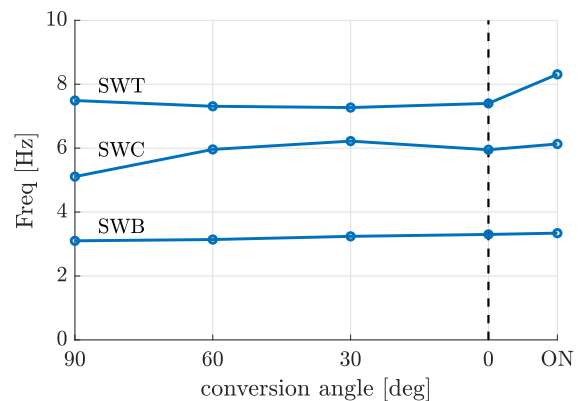Figure 9: Airframe modes vs nacelle angle: Antisymmetric modes

Figure 10: Airframe modes vs nacelle angle: Symmetric modes

Figures 10 and 9 show the frequency trend of the symmetric and antisymmetric wing modes, respectively, as functions of the angle of the nacelle. The change in the stiffness of the downstop with respect to the angle of the

nacelle contributes to the change in frequency: in particular, the SWT mode increases its frequency by almost 1 Hz when the downstop locking mechanism is activated. A detailed validation of the structural model of the XV-15 can be found in [30].

4 TRIM PROCEDURE

Considering an almost symmetric flight condition in airplane mode, the trim problem consists in computing the elevator deflection δ_{el}, the aircraft pitch angle θ, and the collective pitch angle θ_0. Since the trim condition searched is a straight flight condition, it is possible to decouple the rotor trim from the aircraft one.

4.1 AIRCRAFT TRIM

Since the condition is symmetric, the problem reduces to finding the deflection and pitch angle of the elevator that guarantee longitudinal equilibrium. The trim problem in the coupled simulation is initialized by setting an initial elevator deflection and pitch angle of the entire aircraft. Then, to automatically find the static trim point a PID regulator is introduced in the simulation with the aim to bring to zero the vertical reaction force F_z and the pitching moment M_y of the total joint located at the attachment between the wing and the fuselage, by computing δ_E and θ. This point is chosen because it is sufficiently close to the center of mass. Since the objective of the controller is to bring the reaction forces to zero, the most important term in the controller is the integrator $\mathbf{K_I}$:

$$(2) \qquad \begin{Bmatrix} \theta \\ \delta_{el} \end{Bmatrix} = \begin{bmatrix} K_{I\theta} & 0 \\ 0 & K_{I\delta} \end{bmatrix} \begin{Bmatrix} \int T_z \\ \int M_y \end{Bmatrix}$$

A simplified model is used to compute the static trim curves: the lifting surfaces are modeled thought vortex lattice elements with movable surface. In the structural model, the rotors are simplified with a lumped mass element; instead, the flexibility of the wing is considered. To avoid possible interaction between the controller and structural dynamics, a Butterworth second-order low-pass filter with a cutting frequency $\omega_c = 1\,\mathrm{Hz}$ is placed between the reaction forces measure and the regulator. The results of the simulation are shown in Figs. 11–12 for a wind speed of $164.4\,\mathrm{m\,s^{-1}}$. Figure 13 shows the resulting trim variables obtained as a function of the velocity using a simplified DUST vortex lattice model coupled with the MBDyn elastic airframe.
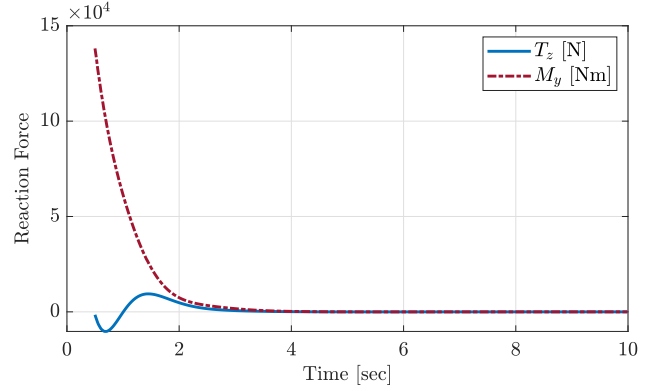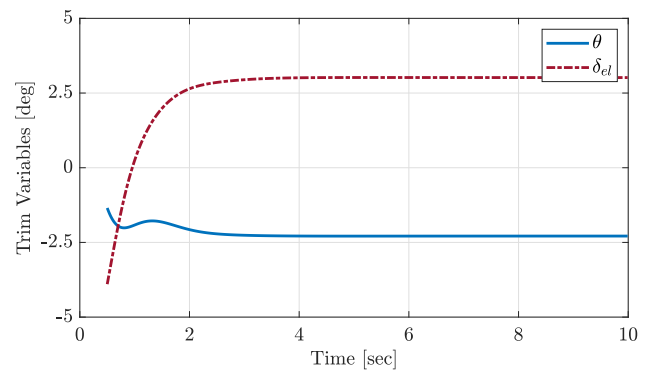

Figure 11: Time history of the reaction forces
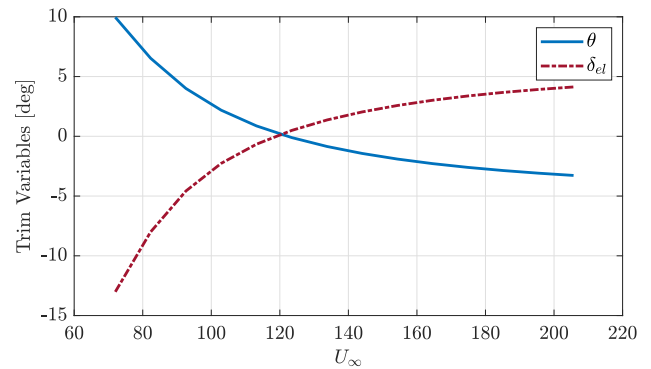

Figure 12: Time history of the trim variables

Figure 13: Trim variables as function of U_∞

4.2 ROTOR TRIM

Rotor trim in airplane configuration is achieved targeting thrust and zero cyclic gimbal flap until maximum torque is reached, maintaining constant rotor speed. At that point, a constant torque trim is maintained to represent a steady powered descent. Power-on trim is achieved by starting from an initial guess of the collective angle with the nominal rotor speed, and then applying the desired torque at the engine side. The desired rotor speed is maintained using a purely integral controller of the kind described in 4 that sets

the appropriate collective head displacement. The wind-mill condition can be achieved simply by setting the applied torque to zero.

Figure 14 presents a comparison between MBDyn and the CAMRAD-JA model of the trim results for the power-on configuration.
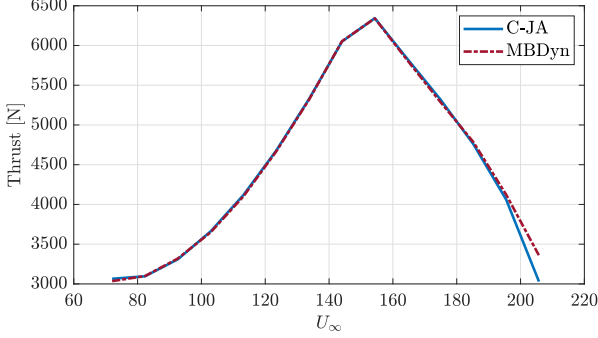

Figure 14: Thrust vs U_∞

4.3 AUTOPILOT

The trim curves shown in Fig. 12 are used only to obtain the trimmed initial condition, whereas during the simulation the task to keep the level flight also when the flight velocity is changed or when the rotorcraft is excited by external disturbances is demanded to the autopilot. As depicted in Fig. 15 the elevator deflection is therefore the sum of two distinct contributions, the trim contribution δ_t and the autopilot contribution δ_p. The autopilot control law is designed starting from the following longitudinal dynamics equilibrium equation for the airframe where the degrees of freedom are altitude z and attitude θ:

(3)
$$m(\ddot{z} + d_{cg}\ddot{\theta}) - L_w - L_t + mg = 0$$

(4)
$$I_{yy}\ddot{\theta} + md_{cg}\ddot{z} + L_w(d_w + d_{cg}) - M_w - L_t(d_t - d_{cg}) - M_t = 0$$

Where m and I_{yy} are the aircraft mass and the pitch inertia moment, d_{cg}, d_t, d_w is the distance between the pole and the center of mass, the wing aerodynamic center and the tail aerodynamic center, L_w and L_t are the lift associated to the wing and horizontal tail plane, M_w and M_t are the aerodynamic moment of wing and tail-plane. The aerodynamic forces are modeled with the classical strip theory model with a Prandlt-Glauert compressibility correction:

(5)
$$L = \frac{\frac{1}{2}\rho U_\infty^2 S C_{L_\alpha} \alpha}{\sqrt{1 - Ma^2}}$$

where C_{L_α} is the slope of the lift coefficient curve and α the angle of attack of the considered part, wing or tail. In the context of this work, the aerodynamic characteristics $C_{L_\alpha}^w$ and $C_{L_\alpha}^t$, for the wing and the tail, respectively, have been computed with DUST, considering the three-dimensional effects and the aerodynamic interaction between the wake of the wing and the horizontal tail.

The angle of attack α can be written in a linearized form as:

(6)
$$\alpha(\theta, \dot{\theta}, \dot{z}) = \alpha_0 - \theta - \frac{\dot{z} + d_w\dot{\theta}}{U_\infty} + \eta\delta_{el}$$

Inserting in equation 4 the expression of equations 5 and 6 and casting the system in state-space from with input the elevator deflection δ_{el} and output the altitude measure, we obtain:

(7)
$$\dot{\mathbf{x}} = \mathbf{Ax} + \mathbf{B}\delta_{el}$$

(8)
$$y = \mathbf{Cx}$$

where $\mathbf{x} = [\dot{z}\ \dot{\theta}\ z\ \theta]^T$ and $y = z$ In fig. 16 the aircraft transfer function is plotted for different air-stream velocities. In order to avoid possible adverse interaction between the structural dynamics and the autopilot, the vertical position z measurement is low-pass filtered using a second order Butterworth filter with a $1\,\mathrm{Hz}$ cut frequency for a wind speed of $144\,\mathrm{m\,s^{-1}}$. The state is therefore increased as: $\mathbf{x} = [\mathbf{x}^T\ \mathbf{x_f}^T]^T$.

To compensate for the initial trimming error of the airplane, due to the flexibility of the wing and the presence of the rotors, an integral action in the autopilot is mandatory. The system is therefore augmented as:

(9)
$$\left\{\begin{matrix}\dot{\mathbf{x}} \\ \dot{x_i}\end{matrix}\right\} = \begin{bmatrix}\mathbf{A} & \mathbf{0} \\ \mathbf{C} & 0\end{bmatrix}\left\{\begin{matrix}\mathbf{x} \\ x_i\end{matrix}\right\} + \begin{bmatrix}\mathbf{B} \\ 0\end{bmatrix}\delta_{el} + \mathbf{w}$$

(10)
$$y_i = \begin{bmatrix}\mathbf{0} & 1\end{bmatrix}\left\{\begin{matrix}\mathbf{x} \\ x_i\end{matrix}\right\} + v$$

Here, $\mathbf{w}$ and v are Gaussian white noises for the process and measurement. The LQG regulator is designed to minimize the cost function:

(11)
$$J = \int_t \left\{\mathbf{x}^T\quad x_i\right\}\mathbf{Q}\left\{\begin{matrix}\mathbf{x} \\ x_i\end{matrix}\right\} + \delta_{el}R\delta_{el}$$

Here $\mathbf{Q}$ and $\mathbf{R}$ are diagonal weight matrices that are needed to adjust the autopilot performance. The LQG regulator is design solving the continuous Riccati equation using the python library `control`.
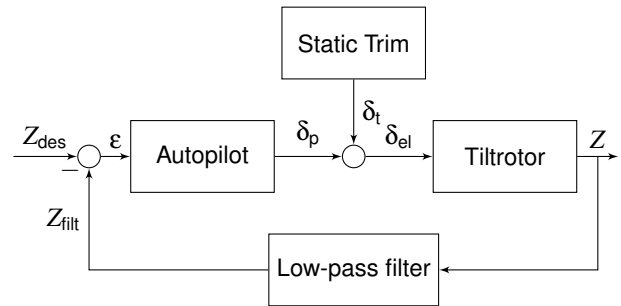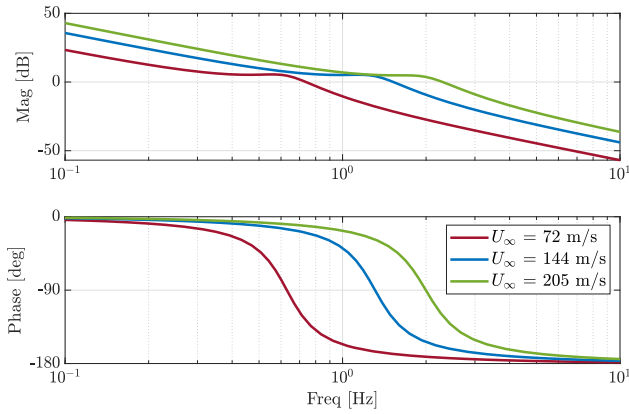

Figure 15: Tiltrotor autopilot loop

Figure 16: Rigid tiltrotor longitudinal dynamics: Bode frequency response

5 PILOT BIOMECHANICAL MODEL

A detailed biomechanical virtual testing environment, based on an original multibody dynamics approach, has been under development by the authors' research group for several years. It comprises the biomechanical representation of the upper limbs, spine and head segments, a compliant seat model that includes unilateral non-linear viscoelastic elements representing the cushions, and rigid bodies representing the inceptors [16]. Three piecewise linear viscoelastic elements are also introduced to model the trim mechanism applied to the inceptors [31] as shown in Fig. 17.
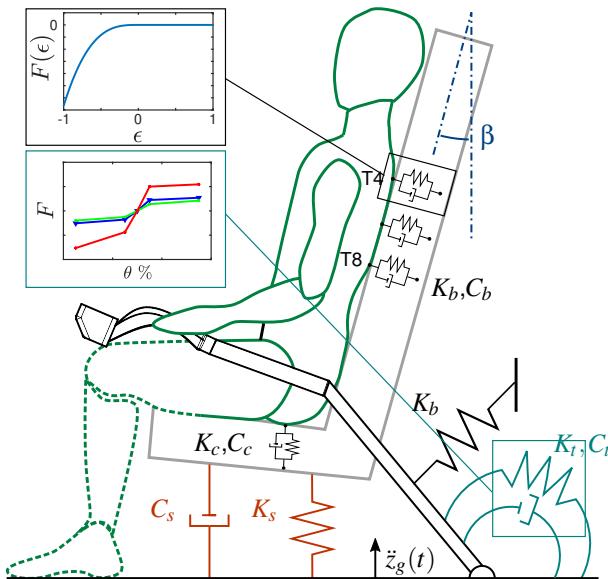

Figure 17: Seat-pilot schematic representation

Muscles in the upper limbs are modeled by nonlinear 1D (rod) viscoelastic elements that reproduce both the passive

and active force contributions, according to a simplified Hill-type muscle model [32]. The muscular activation needed to maintain a static reference pose is computed through a specialized procedure, involving inverse kinematics, inverse dynamics, and optimization steps. The *reflexive* contribution to the total activation, responsible for posture control, is also introduced, considering a quasi-steady approximation of the activation dynamics [16].

Figure 18 represents the connection scheme between the tiltrotor and the pilot. Position, velocity, and acceleration in all 6 degrees of freedom are sent from the seat node located in the tilt-rotor airframe model to the correspondent node located in the pilot model. Then, the rotations of the control inceptors are sent to the rotor swashplate through a gear ratio [33].
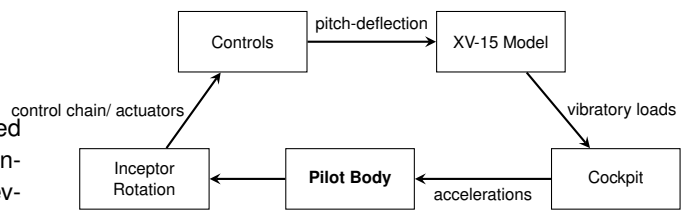

Figure 18: Tiltrotor-pilot loop representation

6 MODAL RESPONSE IDENTIFICATION

To identify the shapes of the airframe mode and modal parameters such as frequency and damping, there exists a wide variety of techniques to excite the aircraft in flight such as impulse, turbulence, or frequency sweep excitation. However, [34] showed that frequency sweep excitation was the most promising approach, less sensitive to noise, and requires less flight time.

To tune the numerical experiments, a simplified model has been used: the blades have been considered as rigid bodies with their aerodynamics modeled using the MBDyn 2D lifting line with a dynamic inflow model [35], whereas for the airframe aerodynamics model the DUST linear vortex lattice elements have been used. To excite structural modes during the simulation, dual flaperon exciters with imposed frequency sweep controls were adopted, allowing the drive of both flaperons to selectively excite symmetric and antisymmetric modes, following the strategy adopted by [17] during flight tests.

Symmetric modes were excited by driving the left and right flaperons in phase, while anti-symmetric modes were excited by driving the flaperons in the opposite phase. A chirp function varying from $2\,\mathrm{Hz}$ to $10\,\mathrm{Hz}$ for the duration of $32\,\mathrm{s}$ has been applied to the flaperon. The starting amplitude is of $2.5\,°$ of flaperon motion, that is linearly decreased with frequency. Figure 19 shows the first $10\,\mathrm{s}$ time history of the flaperon frequency sweep.
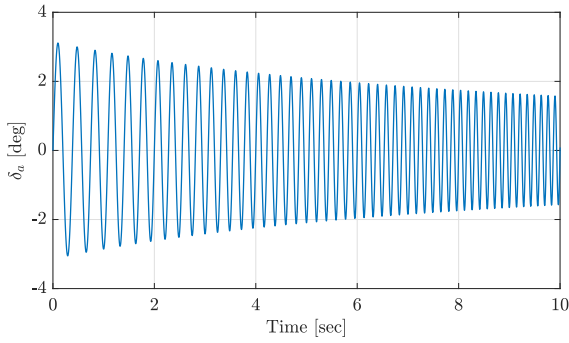
Figure 19: Time history of the flaperon frequency sweep deflection
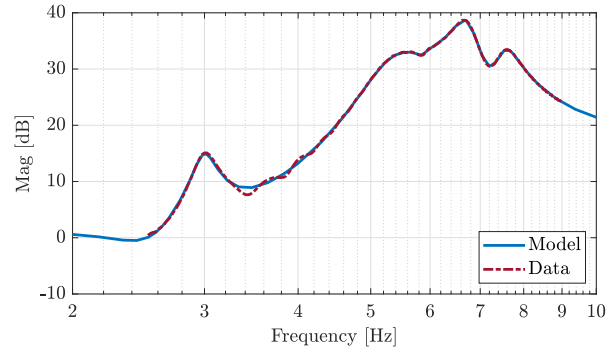

Figure 21: Transfer function of the dynamic model, measured data (blue) and identified model (red)

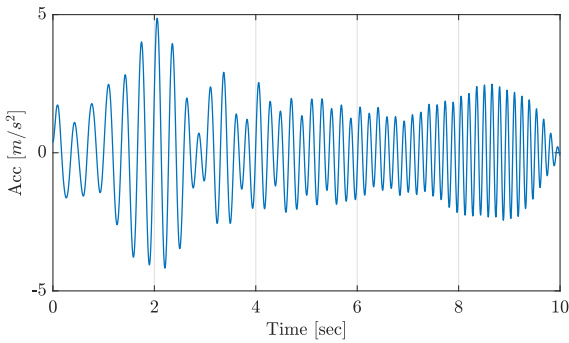The modal parameters extracted are presented in terms of the stabilization diagram in Fig. 22.
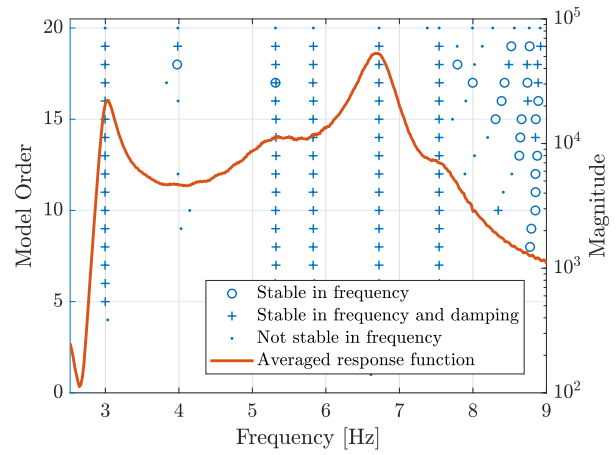

Figure 20: Measured hub vertical acceleration

Figure 22: Stabilization diagram

In Fig. 20 is reported the time history obtained in terms of vertical acceleration measured at the hub node when a symmetric excitation is applied for a wind speed of $144\,\mathrm{m\,s^{-1}}$. The accelerations of the hub as well as the bending and torsional moments of the wing root are used to identify a dynamic model of the system.

The time history is then filtered with a Butterworth second-order low-pass filter with a cutting frequency $\omega_c = 10\,\mathrm{Hz}$. The filtered signals are converted from time-domain into frequency response data by empirical transfer function estimation. The estimated Frequency Response Function (FRF) is then used to identify a state-space model of the tilt-rotor vibration response. A value of $12\,000$ frequency points was used for response computation. The response function is fitted with an iterative nonlinear least-squares refinement, based on the Levenberg-Marquardt search method, of model's parameters. The comparison between the original FRF of the vertical displacement of the hub and the identified model is shown in Fig. 21.

The pilot response is then analyzed. In Fig. 23 is reported the collective variation time history with respect to nominal trim condition at $144\,\mathrm{m\,s^{-1}}$. The maximum variation with respect to the trim condition is just below 4% and from the Bode diagram in Fig. 24 it is clear that this biomechanical mode has a frequency slightly below the first wing bending mode. The second highly visible structural mode is coupled with the collective response.
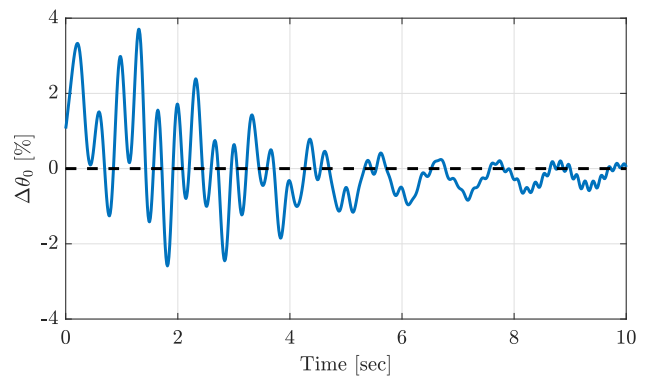

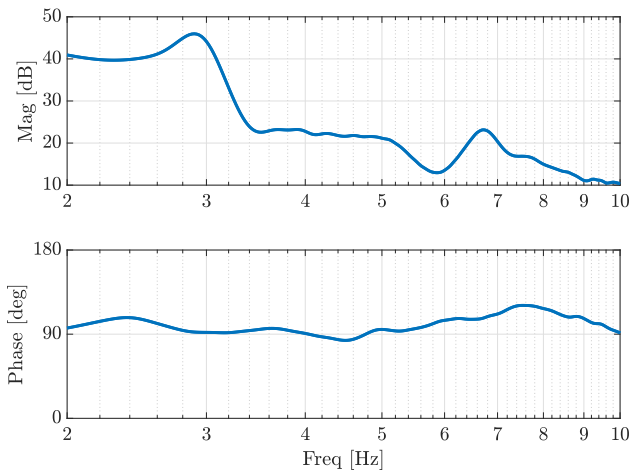Figure 23: Time history of the collective rotation

Figure 24: Aileron to collective rotation transfer function

The same mode is visible in Fig. 25 that represent the transfer function between the aileron deflection and the vertical head acceleration. In this case the second mode is slightly visible in the transfer function.
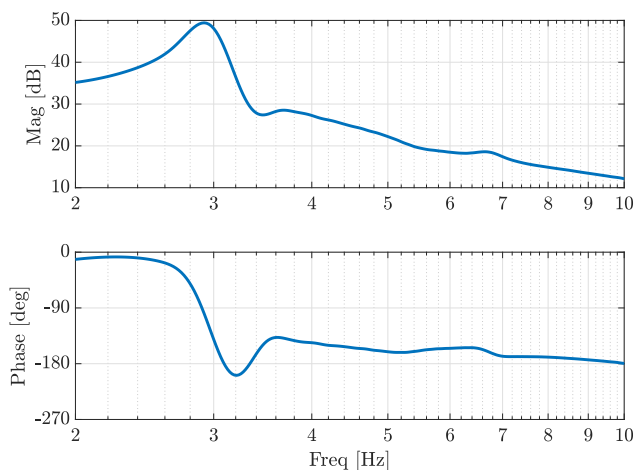

Figure 25: Aileron to pilot head transfer function

7   CONCLUSIONS

The complete aero-servo-elastic model Bell XV-15 tiltrotor equipped with ATB blade has been presented and validated using open-source software MBDyn and DUST. The trim points have been found using a simplified aerodynamic model of the airframe with an integral controller, then the longitudinal free-free condition is controlled through an optimal longitudinal control of the tiltrotor designed using a reduced-order model of the tiltrotor.

Finally, the detailed biomechanical pilot model has been coupled with the aeroelastic tiltrotor model, and the aeroelastic stability is evaluated through a frequency sweep excitation of the model during a time-marching simulation. In this work only the preliminary result of the analysis based on a rigid blade rotor model with a simplified airframe aerodynamics has been presented.

In future work the same procedure will be applied at full elastic rotor model with full unsteady vortex particle aerodynamics. Furthermore, a wide spectrum of different analyses will be possible and performed with this model from passengers' comfort, to performances in transient maneuvers.

Acknowledgments

Copyright Statement

References

[1] Martin D. Maisel, Demo J. Giulianetti, and Daniel C. Dugan. *The History of The XV-15 Tilt Rotor Research Aircraft - From Concept to Flight.* National Aeronautics and Space Administration, Office of Policy and Plans . . . , 2000. NASA SP-2000-4517, Monographs in Aerospace History #17.

[2] Harold Rosenstein and Ross Clark. Aerodynamic development of the V-22 tilt rotor. In *12th European Rotorcraft Forum*, Garmisch-Partenkirchen, Germany, September 22-25 1986.

[3] Tom Parham, Jr. and Lawrence M. Corso. Aeroelastic and aeroservoelastic stability of the BA 609. In *25th European Rotorcraft Forum*, pages G3–1–10, Rome, Italy, September 14–16 1999.

[4] William Fraser, David King, Joseph M. Schaeffer, and Dan Wells. Development of powered-lift airworthiness standards as applied to the AW609 tiltrotor certification basis. In *Proceedings of the 74th Annual Forum of the American Helicopter Society*, Phoenix, AZ, USA, May 14–17 2018.

[5] ACARE — Report of the Group of Personalities. European aeronautics: a vision for 2020, January 2001.

[6] Jiří Čečrdle. Whirl flutter-related certification according to FAR/CS 23 and 25 regulation standards. In *IFASD 2019*, Savannah, Georgia, USA, June 9–13 2019.

[7] Christopher Koch. Parametric whirl flutter study using different modelling approaches. *CEAS Aeronautical Journal*, 2021. doi:10.1007/s13272-021-00548-0.

[8] Mattia Mattaboni, Pierangelo Masarati, and Paolo Mantegazza. Multibody simulation of a generalized predictive controller for tiltrotor active aeroelastic control. *Proc. IMechE, Part G: J. Aerospace Engineering*, 227(1):124–140, January 2013. doi:10.1177/0954410011406203.

[9] M. Mattaboni, P. Masarati, G. Quaranta, and P. Mantegazza. Multibody simulation of integrated tiltrotor flight mechanics, aeroelasticity and control. *J. of Guidance, Control, and Dynamics*, 35(5):1391–1405, September/October 2012. doi:10.2514/1.57309.

[10] Alessandro Cocco, Pierangelo Masarati, Stefan van 't Hoff, and Bart Timmerman. Numerical whirl-flutter analysis of a tiltrotor semi-span wind tunnel model. *CEAS Aeronautical Journal*, in press. doi:10.1007/s13272-022-00605-2.

[11] Jr. C. W. Acree. An improved CAMRAD model for aeroelastic stability analysis of the XV-15 with advanced technology blades. TM 4448, NASA, 1993.

[12] C. W. Acree, R. J. Peyran, and Wayne Johnson. Rotor design options for improving tiltrotor whirl-flutter stability margins. *Journal of the American Helicopter Society*, 46(2):87–95, April 2001. doi:10.4050/JAHS.56.022004.

[13] Pierangelo Masarati, Marco Morandini, and Paolo Mantegazza. An efficient formulation for general-purpose multibody/multiphysics analysis. *J. of Computational and Nonlinear Dynamics*, 9(4):041001, 2014. doi:10.1115/1.4025628.

[14] Matteo Tugnoli, Davide Montagnani, Monica Syal, Giovanni Droandi, and Alex Zanotti. Mid-fidelity approach to aerodynamic simulations of unconventional VTOL aircraft configurations. *Aerospace Science and Technology*, 115:106804, 2021.

[15] Alberto Savino, Alessandro Cocco, Alex Zanotti, Matteo Tugnoli, Pierangelo Masarati, and Vincenzo Muscarello. Coupling mid-fidelity aerodynamics and multibody dynamics for the aeroelastic analysis of rotary-wing aircraft configurations. *Energies*, 14(21):6979, 2021. doi:10.3390/en14216979.

[16] Andrea Zanoni, Alessandro Cocco, and Pierangelo Masarati. Multibody dynamics analysis of the human upper body for rotorcraft–pilot interaction. *Nonlinear Dynamics*, 102(3):1517–1539, 2020. doi:10.1007/s11071-020-06005-7.

[17] Cecil W Acree Jr and Mark B Tischler. Identification of xv-15 aeroelastic modes using frequency-domain methods. Technical report, 1989.

[18] Abhineet Gupta, Peter J Seiler, and Brian P Danowsky. Ground vibration tests on a flexible flying wing aircraft-invited. In *AIAA atmospheric flight mechanics conference*, pages 17–53, 2016.

[19] Huimin Zhang, Runsen Zhang, Andrea Zanoni, and Pierangelo Masarati. Performance of implicit A-stable time integration methods for multibody system dynamics. *Multibody System Dynamics*, 54(3):263–301, 2022. doi:10.1007/s11044-021-09806-9.

[20] G. S. Winckelmans. *Topics in vortex methods for the computation of three-and two-dimensional incompressible unsteady flows*. Ph.D. dissertation, California Institute of Technology, 1989.

[21] G. H. Cottet and P. D. Koumoutsakos. *Vortex methods: theory and practice*. Cambridge University Press, 2000.

[22] L. Morino and C.-C. Kuot. Subsonic potential aerodynamics for complex configurations: A general theory. *AIAA Journal*, 12(2):191–197, 1974. doi:10.2514/3.49191.

[23] Matteo Tugnoli, Davide Montagnani, Monica Syal, Giovanni Droandi, and Alex Zanotti. Mid-fidelity approach to aerodynamic simulations of unconventional vtol aircraft configurations. *Aerospace Science and Technology*, 115:106804, 2021.

[24] Gian Luca Ghiringhelli, Pierangelo Masarati, and Paolo Mantegazza. A multi-body implementation of finite volume C^0 beams. *AIAA Journal*, 38(1):131–138, January 2000. doi:10.2514/2.933.

[25] Olivier A. Bauchau, Peter Betsch, Alberto Cardona, Johannes Gerstmayr, Ben Jonker, Pierangelo Masarati, and Valentin Sonneville. Validation of flexible multibody dynamics beam formulations using benchmark problems. *Multibody System Dynamics*, 37(1):29–48, 2016. doi:10.1007/s11044-016-9514-y.

[26] RB Lehoucq and JA Scott. An evaluation of software for computing eigenvalues of sparse nonsymmetric matrices. *Preprint MCS-P547*, 1195(5), 1996.

[27] P. Masarati. Direct eigenanalysis of constrained system dynamics. *Proc. IMechE Part K: J. Multi-body Dynamics*, 223(4):335–342, 2009. doi:10.1243/14644193JMBD211.

[28] Fort F. Felker, Larry A. Young, and David B. Signor. Performance and loads data from a hover test of a full-scale advanced technology XV-15 rotor. TM 86854, NASA, 1986.

[29] Vincenzo Muscarello, Francesca Colombo, Giuseppe Quaranta, and Pierangelo Masarati. Aeroelastic rotorcraft-pilot couplings in tiltrotor aircraft. *J. of Guidance, Control, and Dynamics*, 42(3):524–537, 2019. doi:10.2514/1.G003922.

[30] Alessandro Cocco, Alberto Savino, and Pierangelo Masarati. Flexible multibody model of a complete tiltrotor for aeroservoelastic analysis. In *ASME IDETC/CIE 2022*, St. Louis, Missouri, USA, August 14–17 2022. doi:10.1115/DETC2022-88973.

[31] Andrea Zanoni, Alessandro Cocco, Vincenzo Muscarello, and Pierangelo Masarati. Effects of flight controls and cockpit layout design in rotorcraft-pilot couplings: a computational approach. In *ASME IDETC/CIE 2020*, St. Louis, MO, USA (virtual), 2020. doi:10.1115/DETC2020-22304.

[32] E. Pennestrì, R. Stefanelli, P. P. Valentini, and L. Vita. Virtual musculo-skeletal model for the biomechanical analysis of the upper limb. *Journal of Biomechanics*, 40(6):1350–1361, 2007. doi:10.1016/j.jbiomech.2006.05.013.

[33] S. W. Ferguson, W. F. Clement, W. B. Cleveland, and D. L. Key. Assessment of simulation fidelity using measurements of piloting technique in flight. In *American Helicopter Society 40th Annual Forum*, pages 67–92, Arlington, VA, USA, May 16–18 1984.

[34] M TISCHLER, J LEUNG, and D DUGAN. Frequency-domain identification of xv-15 tilt-rotor aircraft dynamics. In *2nd Flight Testing Conference*, page 2695, 1983.

[35] Dale M. Pitt and David A. Peters. Theoretical prediction of dynamic-inflow derivatives. *Vertica*, 5(1):21–34, 1981.